SCIENTIFIC REPORTS

OPEN

SUBJECT AREAS:
ELECTRONIC STRUCTURE
ELECTRONIC PROPERTIES AND MATERIALS
DENSITY FUNCTIONAL THEORY

Received
26 February 2014

Accepted
4 June 2014

Published
24 June 2014

Correspondence and requests for materials should be addressed to H.S. (hbsu@ntu.edu.sg)

Cuprate-like Electronic Properties in Superlattices with $Ag^{II}F_2$ Square Sheet

Xiaoping Yang & Haibin Su

Institute of Advanced Studies, Nanyang Technological University, 50 Nanyang Avenue, 639798 Singapore.

Using the generalized gradient approximation augmented with maximally localized Wannier functions analysis, we present the formation of cuprate-like electronic structures in $Ag^{II}F_2$–related superlattices resulted from the confinement together with structural chemical modification. The out–of–plane electronic reconstruction leads to electron doping of AgF_2 plane and gradually destablizes the antiferromagnetic state. Eventually a stable nonmagnetic metallic state emerges by applying in–plane tensile strain, in which the shape of effective Fermi surface of AgF_2 plane exhibits the key feature of high–temperature cuprate superconductor.

The discovery of high–temperature superconductivity in cuprates[1] initiated the quest for exploring superconductivity in other transition-metal compounds. Ag^{2+} is isoelectronic with Cu^{2+} (d^9 configuration). F^- and O^{2-} are also isoelectronic ions, closed–shell species, moreover both F^- and O^{2-} are weak–field ligands. Given the existence of the superconducting cuprates, one might be naturally interested in searching the superconductivity in Ag^{2+}–F^- solids. Theoretical study[2–4] of Grochala and Hoffmann has also suggested that properly hole–or electron–doped Ag^{II} fluorides might be good superconductors, due to similarity in structure and properties between the Ag^{II} fluorides and the cuprate superconductors. Particularly, Jaron and Grochala have predicted that the high pressure σ form of AgF_2 compound (>15 GPa) is a layered material with antiferromagnetic (AFM) ordering[4], as seen for the parent compounds of high–temperature cuprate superconductors[5].

It is well known that $[CuO_2]\infty$ plane with tetragonal tetra coordination of Cu (weak apical Cu–O bonds), is an essential structural element for superconductivity in cuprates. The basic band structure of the doped cuprates is a single 2D Cu–$d_{x^2-y^2}$ —like band deviating from half filled. In this situation, AFM fluctuations prevail in the undoped parent compounds and are often believed to mediate the superconductivity. The Fermi surface (FS) from this $d_{x^2-y^2}$ band has been observed in many overdoped cuprates and agrees with the density functional theory based band structure calculations[5,6].

As Grochala and Hoffmann pointed out in their review paper[2], analogous $[AgF_2]\infty$ plane with tetracoordinate Ag has not been reported experimentally. Noteworthy recent development of heterostructure interface technology, superlattices (SLs) containing $Ag^{II}F_2$ square lattices can be prepared by using appropriate synthetic techniques to incorporate alternating layers of different transition metal compounds[7–14], even technically a single atomic layer[11]. Here, interface can be used to modulate electronic structure for manipulating physical properties and generating novel phases which are not present in the bulk constituents. Whereby the quest for Ag^{II} superconductors could be achieved by the aforementioned novel paradigm on designing and fabricating two dimensional materials[15–18]. In our paper, our research focuses on artificial superlattice materials design and their electronic properties and doping effects, different from research on real bulk Ag^{II} fluorides materials[2–4].

To identify possible superconductivity in 2D Ag^{2+}–F^- square sheet, we investigate electronic structures, magnetic states, model hamiltonian parameters and effective FSs for three proposed superlattices: $SrTiO_3$/AgF_2 (STO/AgF_2), $BaTiO_3$/AgF_2 (BTO/AgF_2) and $SrTiO_3$/$CsAgF_3$ (STO/$CsAgF_3$), as illustrated in the top panels of Fig. 1, and compare these with corresponding properties of the cuprate superconductors. We find cuprate-like band structures and strong AFM fluctuations in all these SLs. More importantly, large cation size increases cation–anion polarization strength and corresponding apical Ag–O/F distance, and makes oxygen band edge shift above the Fermi level to exchange charge with Ag–$d_{x^2-y^2}$ band, leading to out–of–plane electronic reconstruction. Here, similar to charge transfer in cuprates and recently studied La_2CuO_4–related heterostructure[18], the TiO_2 plane actually serves as a charge reservoir block and transfer electrons to the AgF_2 plane. As a result, AFM state presents an unstable trend. Finally, the applied in–plane tensile strain drives a novel phase transition from the AFM metallic state to a stable nonmagnetic (NM) metallic state in STO/$CsAgF_3$ SL. Model hamiltonian

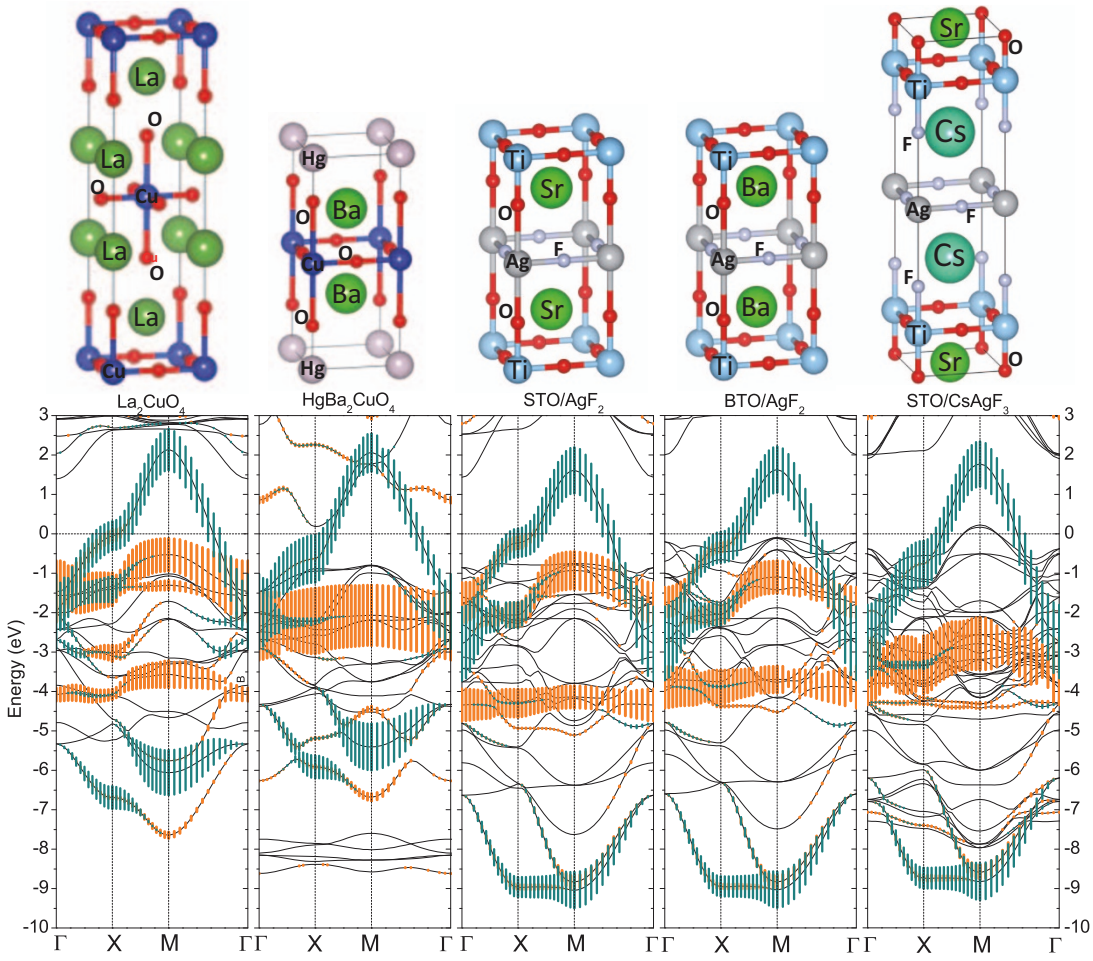

Figure 1 | Schematic geometrical structures and GGA bandstructures of bulk LCO, bulk HBCO, STO/AgF_2, BTO/AgF_2 and STO/$CsAgF_3$ SLs from left to right. The Fermi level ε_F is set at zero. Dark cyan and orange fatbands represent contribution of $d_{x^2-y^2}$ and d_{3z^2-1} orbitals respectively.

parameters and FS character of STO/$CsAgF_3$ are extracted and compared to La_2CuO_4 (LCO) and $HgBa_2CuO_4$ (HBCO), indicating that STO/$CsAgF_3$ is a promising candidate for Ag^{II} superconductivity.

Results

For the in–plane lattice constant a of SLs, we first took that of STO (3.905 Å), often used as the substrate. The lattice constant c and atomic z coordinates were fully relaxed. The main effect of the relaxation, is to make the negatively charged O/F and positively charged cations displaced relative to each other in SrO, BaO and CsF atomic layers, and thereby polarize the cation and anion planes. Cation size affects significantly polarization strength and corresponding apical Ag–O(F) bond length. AgF_2 layer acts as the mirror plane of whole unit cell. In STO/AgF_2 and BTO/AgF_2 SLs, oxygen atoms move symmetrically towards and against AgF_2 plane by 0.077 Å and 0.064 Å respectively. As a result, apical Ag–O bond length in the BTO/AgF_2 is slightly larger than that in the STO/AgF_2 by 0.143 Å, due to the larger size of the Ba^{2+} cation. The largest cation–anion polarization occurs in CsF plane in the STO/$CsAgF_3$, and is 0.623 Å against AgF_2 plane. This polarization distortion produces a local ionic dipole moment, and together with in–plane strain it also leads to a larger increment in the apical Ag–F distance ($d^{apical}_{Ag-F}=3.405$ Å) compared to apical Ag–O distance ($d^{apical}_{Ag-O}=2.486$, 2.629 Å) in other two SLs.

Local ionic dipole moment perturbs electrostatic potential and changes band positions around the Fermi Level. An evolution of Ag-e_g states with structural chemical modification can be clearly observed in band structures. Spin–polarized GGA calculations give paramagnetic ground state for all these superlattices. Fig. 1 shows energy bands of STO/AgF_2, BTO/AgF_2 and STO/$CsAgF_3$ SLs in a 13 eV region around the Fermi level $\varepsilon_F \equiv 0$ and along the symmetry–lines $\Gamma-X-M-\Gamma=(0,0,0)-\left(\frac{\pi}{a},0,0\right)-\left(\frac{\pi}{a},\frac{\pi}{a},0\right)-(0,0,0)$. The energy bands of bulk LCO and HBCO are also plotted in Fig. 1 for comparison. For three SLs, electronic properties around ε_F are still mainly controlled by Ag-e_g bands, which are above the filled O/F-2p and Ag-t_{2g} bands, and below the empty Ti-3d bands. We plot $d_{x^2-y^2}$ (dark cyan) and d_{3z^2-1} (orange) fatbands around ε_F to disclose their orbital contribution. Ag-e_g antibonding bands have similar band width in superlattice configuration STO/AgF_2 and BTO/AgF_2, and resemble that of LCO. Note that oxygen 2p bands become closer to Fermi Level in BTO/AgF_2 due to atomic polarization distortion in z direction. However, in STO/$CsAgF_3$ case, the antibonding band between Ag–d_{3z^2-1} and F-p states disappears due to the weak mixing of Ag-3d and F-p states in z direction. As a result, e_g bands from −4 to 2 eV looks more like that of HBCO with a larger apical Cu-O distance of 2.784 Å. Most importantly, oxygen 2p band edge of TiO_2 plane upshifts eventually above the Fermi level and exchanges charge with Ag–$d_{x^2-y^2}$ band, as seen in layer–projected density of states in the left panel of Fig. 2.

In order to investigate the microscopic orbital physics of polarization–induced electron doping, we plot the typical partial charge density of the unoccupied bands of STO/$CsAgF_3$ from Fermi level to 0.25 eV in the right panel of Fig. 2. Obviously, electron doping originates from charge transfer between O-p_x,p_y orbitals at TiO_2

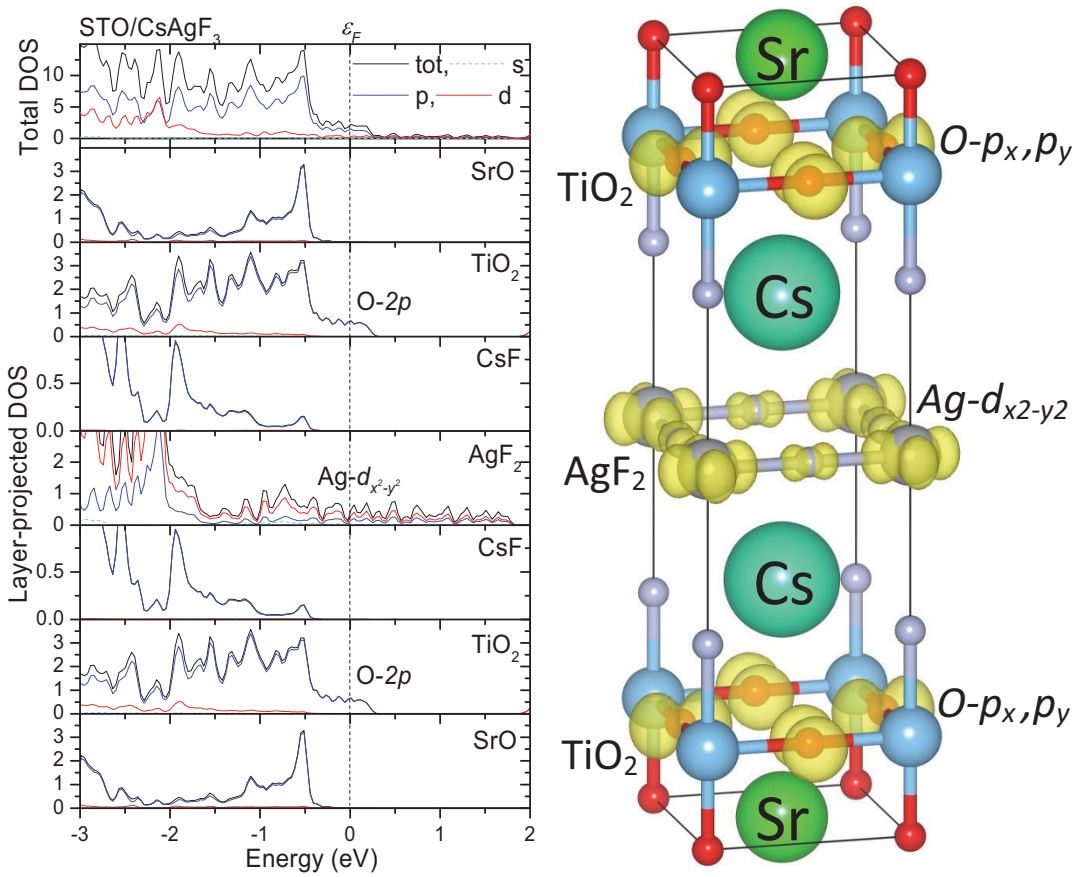

Figure 2 | Layer–projected density of states (left panel) of STO/$CsAgF_3$ SL, and corresponding partial charge density isosurfaces (right panel) for the unoccupied bands from Fermi level to 0.25 eV.

interface and Ag–$d_{x^2-y^2}$ orbital. Here, Ag–$d_{x^2-y^2}$ has considerable covalent hybridization with in–plane fluorine atoms' p_x, p_y orbitals, similar to Cu^{2+}–O^{2-} bonds. Interestingly, O-p_x,p_y state around the Fermi level is mainly located at TiO_2 interface and far away from the AgF_2 plane, as illustrated in Fig. 2, which favors the realization of possible superconductivity in 2D $Ag^{II}F_2$ plane.

Next, we discuss the stability of magnetic states in three superlattices under GGA + U_d scheme. AFM band structures with Ag–e_g orbitals character (see Fig. 1 of supplementary materials) indicate that STO/AgF_2 SL presents an AFM insulating ground state with a energy gap of 0.45 eV. While in BTO/AgF_2 electronic correlation drives a weak electron doping in Ag–$d_{x^2-y^2}$ state, which is absent in GGA bands, leading to an insulator–metal transition. For STO/$CsAgF_3$, an AFM metallic ground state is obtained. By analyzing layer–projected density of states of STO/$CsAgF_3$ from GGA + U_d calculations and corresponding partial charge density isosurfaces for the bands around Fermi level (see Fig. 2 of supplementary materials), we find that the obtained AFM metallic ground state is aroused by

Table I | The in–plane and apical bond length $d^{in-plane}_{Ag(Cu)-F(O)}$ and $d^{apical}_{Ag(Cu)-F(O)}$ in Å, energy differences E_{NM}-E_{AFM} in meV/Ag(Cu), and Ag/Cu atom's magnetic moment of AFM state in μ_B/Ag(Cu), for LCO, HBCO, STO/AgF_2, BTO/AgF_2 and STO/$CsAgF_3$ without (top subtable) and with (bottom subtable) in–plane strain

	LCO	HBCO	$\frac{STO}{AgF_2}$	$\frac{BTO}{AgF_2}$	$\frac{STO}{CsAgF_3}$
$d^{in-plane}_{Ag(Cu)-F(O)}$	1.894	1.941	1.953	1.953	1.953
$d^{apical}_{Ag(Cu)-F(O)}$	2.429	2.784	2.486	2.629	3.405
E_{NM}-E_{AFM}	206.510	117.470	91.160	34.525	4.105
Moment	0.542	0.495	0.513	0.403	0.184

		$\frac{STO}{CsAgF_3}$	
$d^{in-plane}_{Ag-F}$	1.895	2.003	2.053
d^{apical}_{Ag-F}	3.760	3.368	3.289
E_{NM}-E_{AFM}	7.595	0.335	*
Moment	0.212	0.102	*

*The instability occurs to the AFM state.

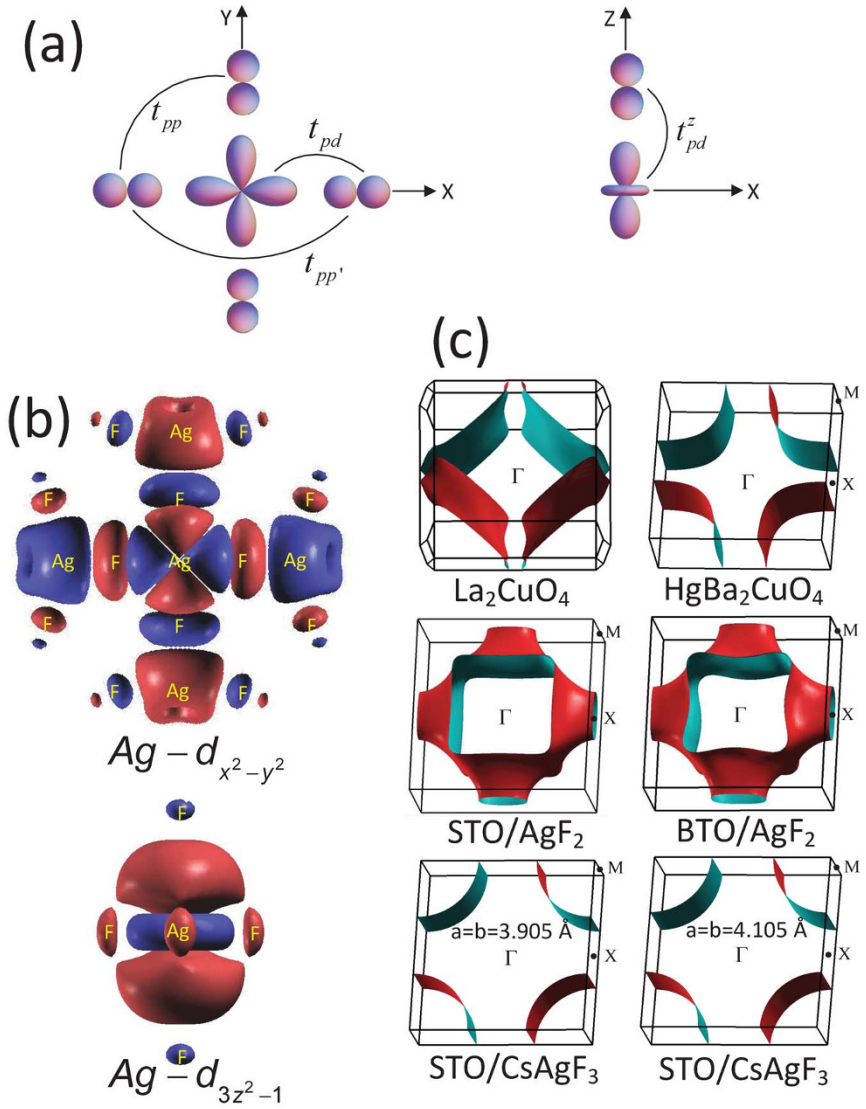

Figure 3 | (a) Parameters of the six–band *p-d* model for the CuO and AgF(O) octahedral in cuprate superconductors and the proposed AgF_2–related superlattices; (b) Localized Wannier functions of $Ag-d_{x^2-y^2}$ and $-d_{3z^2-1}$ orbitals in $STO/CsAgF_3$; (c) Effective Fermi surface centered at Γ point in first Brillouin Zone from $d_{x^2-y^2}$ band for bulk LCO, bulk HBCO, STO/AgF_2, BTO/AgF_2 and $STO/CsAgF_3$ SLs.

charge transfer between O-p_x,p_y orbitals in TiO_2 plane and covalent hybrid orbitals of Ag-$d_{x^2-y^2}$ and F-p_x,p_y in AgF_2 plane. In all three superlattices, FM state falls in between AFM and NM states in energy. In Table I, we summarize in–plane and apical bond lengths $d^{in-plane}_{Ag(Cu)-F(O)}$ and $d^{apical}_{Ag(Cu)-F(O)}$, energy difference E_{NM}-E_{AFM}, and magnetic moment on Ag/Cu atom in AFM state. With the increasing apical Ag-O/F distance, E_{NM}-E_{AFM} value decreases gradually from 91.160 meV/Ag for STO/AgF_2 to 34.525 meV/Ag for BTO/AgF_2, similar to the trend for cuprates (*e.g.* from 206.51 meV/Cu for LCO to 117.47 meV/Cu for HBCO in Table I), and finally to a much smaller value 4.105 meV/Ag in $STO/CsAgF_3$. The process of AFM state instability is also companied by reduction of magnetic moment on Ag/Cu atoms. For superlattice structures, electron doping of AgF_2 plane emerges with the change of apical Ag-O/F distance, as we discussed above, which is an important derivation of AFM state instability, especially in $STO/CsAgF_3$ with much smaller E_{NM}-E_{AFM} value and magnetic moment of 0.184 μ_B/Ag.

Furthermore, we investigate the effect of in–plane strain on magnetic state, because electronic properties are subject to electron– and orbital–lattice couplings in perovskite–like materials. Similar calculations are made for $STO/CsAgF_3$ with three additional in–plane lattice constants of 3.790, 4.005 and 4.105 Å. We find that compressive strain can effectively increase E_{NM}-E_{AFM} to 7.595 meV/Ag, but tensile strain decreases it to 0.335 meV/Ag for a = 4.005 Å. Extraordinarily, $STO/CsAgF_3$ SL goes through phase transition to a stable NM metallic ground state under tensile strain a = 4.105 Å, suggesting that the tuning of in–plane lattice constant can serve as an effective tool to modulate magnetic properties and even superconductivity.

We know that effective low–energy hamiltonians containing the minimal set of bands are important tools for understanding chemical trends. Based on the aboved GGA simulations, we extract model hamiltonian parameters by MLWFs downfolding technique. In this work, we choose to downfold to a 6-band hamiltonian describing the in-plane $d_{x^2-y^2}$, p_x, p_y orbitals, and out–of–plane d_{3z^2-1}, two p_z orbitals (see Fig. 3a). In particular, six parameters capture the essential physics: the e_g crystal field splitting energy $\Delta_1 = \varepsilon_{x^2-y^2} - \varepsilon_{3z^2-1}$, the in–plane charge–transfer energy $\Delta_2 = \varepsilon_{x^2-y^2} - \varepsilon_{p_{x(y)}}$, the direct in–plane and out–of–plane Ag-F (Cu-O) hopping t_{pd} and t^z_{pd}, and the two shortest–ranged O-O hoppings t_{pp}, and $t_{pp'}$. The extracted values are tabulated in Table II, and corresponding interpolated band structure are shown in Fig. 3 of supplementary materials.

Table II | Tight–binding parameters of the six–band *p-d* model, containing the in–plane $d_{x^2-y^2}$, p_x, p_y orbitals and out–of–plane d_{3z^2-1}, p_z orbitals for LCO, HBCO, STO/AgF_2, BTO/AgF_2 and STO/$CsAgF_3$ without (top subtable) and with (bottom subtable) in–plane strain. Parameters include e_g crystal field splitting energies $\Delta_1 = \varepsilon_{x^2-y^2} - \varepsilon_{3z^2-1}$, charge–transfer energies $\Delta_2 = \varepsilon_{x^2-y^2} - \varepsilon_{p_{x(y)}}$, the three nearest–neighbor (intra–cell) hoppings t_{pd}, t_{pd}^z, t_{pp}, and the inter–cell oxygen–oxygen hopping $t_{pp'}$. The in–plane and apical bond lengths $d_{Ag(Cu)-F(O)}^{in-plane}$ and $d_{Ag(Cu)-F(O)}^{apical}$ in Å are also listed

	LCO	HBCO	$\frac{STO}{AgF_2}$	$\frac{BTO}{AgF_2}$	$\frac{STO}{CsAgF_3}$
$d_{Ag(Cu)-F(O)}^{in-plane}$	1.894	1.941	1.953	1.953	1.953
$d_{Ag(Cu)-F(O)}^{apical}$	2.429	2.784	2.486	2.629	3.405
Δ_1	0.005	0.115	0.268	0.324	0.810
Δ_2	2.305	1.476	3.703	3.729	3.504
t_{pd}	1.395	1.249	1.766	1.759	1.755
t_{pd}^z	0.458	0.391	0.972	0.830	0.223
t_{pp}	0.656	0.620	0.391	0.398	0.432
$t_{pp'}$	0.191	0.225	0.089	0.091	0.118

		$\frac{STO}{CsAgF_3}$	
$d_{Ag-F}^{in-plane}$	1.895	2.003	2.053
d_{Ag-F}^{apical}	3.760	3.368	3.289
Δ_1	1.098	0.654	0.520
Δ_2	3.968	3.122	2.785
t_{pd}	1.979	1.583	1.431
t_{pd}^z	0.141	0.227	0.245
t_{pp}	0.479	0.397	0.364
$t_{pp'}$	0.141	0.104	0.092

The hopping integrals t_{pd} and t_{pp} of LCO and HBCO are in good agreement with the 3–band model results by Weber *et al.*[30]. While Δ_2 and $t_{pp'}$ are further corrected in our model by including three additional out–of–plane orbitals. From Table II, we find that cuprates and $Ag^{II}F_2$–related SLs share some common features. The larger $d_{Ag-F(O)}^{apical}$ or d_{Cu-O}^{apical} value leads to the increasing Δ_1 and decreasing out–of–plane hopping t_{pd}^z respectively. And Δ_2, in–plane hoppings t_{pd} and t_{pp} increase with the decreasing $d_{Ag-F}^{in-plane}$ (see bottom subtable) or $d_{Cu-O}^{in-plane}$ respectively. However, in–plane hopping $t_{pp'}$ is an exception, and is affected considerably by out–of–plane Cu–O distance. From LCO to HBCO, the weakened electrostatic repulsion enhanced the hopping $t_{pp'}$ by 0.034 eV when the negatively-charged apical oxygen moves against the CuO plane, although $d_{Cu-O}^{in-plane}$ increases from 1.894 to 1.941 Å at the same time. The similar feature can be seen more clearly in three SLs with the fixed $d_{Ag-F}^{in-plane}$ of 1.953 Å. $t_{pp'}$ changes from 0.089 eV to 0.091 eV, and finally 0.118 eV with the increasing apical Ag–O/F distance. Compared to cuprates, generally STO/$CsAgF_3$ has relatively larger Δ_1, Δ_2, and in–plane Ag–F hopping t_{pd}, while hopping t_{pd}^z, t_{pp} and $t_{pp'}$ are smaller. After applying in–plane tensile strain $d_{Ag-F}^{in-plane} = 2.003$, 2.053 Å (see bottom subtable), one can find that parameters evolve towards those in cuprates, except for t_{pp} and $t_{pp'}$.

In Fig. 3b, we plot the localized Wannier functions of Ag–$d_{x^2-y^2}$ and $-d_{3z^2-1}$ in STO/$CsAgF_3$ SL. Both look like those of cuprates, and have a strong *p-d* covalent hybridization characteristic. Ag–d_{3z^2-1} is more localized due to the big apical Ag–F distance (>3 Å). The FSs centered at Γ point for LCO and HBCO are shown in the first row of Fig. 3c. Compared to LCO (transition temperature T_c = 40 K), the FS of HBCO (T_c = 90 K) has the typical shape of high-T_c cuprates superconductor with constant–energy surface obviously bulging toward Γ point. The FS shape of STO/AgF_2 and BTO/AgF_2 (see the second row of Fig. 3c) is far away from that of HBCO or LCO. However, for STO/$CsAgF_3$ (the third row of Fig. 3c) with polarized electron–doping in AgF_2 plane, effective FSs from Ag–$d_{x^2-y^2}$ band presents the considerable similarity to that of HBCO.

Discussion

We analyze the cuprate-like electronic structures and strong AFM fluctuations in the proposed superlattice with 2D $Ag^{II}F_2$ square sheet. Atomic polarization induces out–of–plane electronic reconstruction occurring between O-p_x,p_y orbitals in TiO_2 plane and covalent hybrid orbitals of Ag–$d_{x^2-y^2}$ and F-p_x,p_y in AgF_2 plane, which is an important origin of AFM state instability. A stable NM metallic ground state emerges in STO/$CsAgF_3$ SL subjected to in–plane tensile strain, meanwhile corresponding Wannier functions of Ag–$d_{x^2-y^2}$, Ag–d_{3z^2-1}, and FS shape present considerable similarity to those in cuprates with the high–T_c. Therefore, d^9 $Ag^{II}F_2$–related superlattices are promising because their physics contains the main ingredients of high–temperature superconductivity.

Method

We carried out the numerical calculations using the Vienna *ab initio* Simulation Package (VASP)[19–22] within the framework of the generalized gradient approximation (GGA) (Perdew-Burke-Ernzerhof exchange correlation functional)[23], and recently developed maximally localized Wannier functions (MLWFs) downfolding technique[24–26]. The ion–electron interaction was modeled by the projector augmented wave (PAW) method[27,28] with a uniform energy cutoff of 500 eV. Spacing between *k* points was 0.02 $Å^{-1}$. The structures of the SLs were optimized by employing the conjugate gradient technique, and in the final geometry, no force on the atoms exceeded 0.01 eV/Å. For magnetic states calculations, we used U_d = 7.5 eV and J_d = 0.98 eV for Ag-*d* and Cu-*d* states[29].

1. Bednorz, J. G. & Müller, K. A. Possible high T_c superconductivity in the Ba–La–Cu–O system. *Z. Phys. B* **64**, 189–193 (1986).
2. Grochala, W. & Hoffmann, R. Real and Hypothetical intermediate–valence Ag^{II}/Ag^{III} and Ag^{II}/Ag^{I} fluoride systems as potential superconductors. *Angew. Chem. Int. Ed.* **40**, 2742–2781 (2001).
3. Grochala, W., Egdell, R. G., Edwards, P. P., Mazej, Z. & Zemva, B. On the covalency of silver–fluorine bonds in compounds of silver(I), silver(II) and silver(III). *ChemPhysChem* **4**, 997–1001 (2003).

4. Jaron, T. & Grochala, W. Prediction of giant antiferromagnetic coupling in exotic fluorides of Ag^{II}. *Phys. Stat. Sol. (RRL)* **2**, 71–73 (2008).
5. Armitage, N. P., Fournier, P. & Greene, R. L. Progress and perspectives on electron-doped cuprates. *Rev. Mod. Phys.* **82**, 2421–2487 (2010).
6. Andersen, O. K., Liechtenstein, A. I., Jepsen, O. & Paulsen, F. LDA energy bands, low–energy hamiltonians, t′, t″, $t_{\perp}^{(k)}$, and $J_{\perp}$. *J. Phys. Chem. Solids* **56**, 1573–1591 (1995).
7. Ohtomo, A. & Hwang, H. Y. A high–mobility electron gas at the $LaAlO_3/SrTiO_3$ heterointerface. *Nature* **427**, 423–426 (2004).
8. Thiel, S., Hammerl, G., Schmehl, A., Schneider, C. W. & Mannhart, J. Tunable quasi–two–dimensional electron gases in oxide heterostructures. *Science* **313**, 1942–1945 (2006).
9. Reyren, N. *et al*. Superconducting interfaces between insulating oxides. *Science* **317**, 1196–1199 (2007).
10. Huijben, M., Brinkman, A., Koster, G., Rijnders, G., Hilgenkamp, H. & Blank, Dave H. A. Structure–property relation of $SrTiO_3/LaAlO_3$ interfaces. *Adv. Mater.* **21**, 1665–1677 (2009).
11. Jang, H. W. *et al*. Metallic and insulating oxide interfaces controlled by electronic correlations. *Science* **331**, 886–889 (2011).
12. Bozovic, I., Logvenov, G., Verhoeven, M. A. J., Caputo, P., Goldobin, E. & Geballe, T. H. No mixing of superconductivity and antiferromagnetism in a high–temperature superconductor. *Nature* **422**, 873–875 (2003).
13. Logvenov, G., Gozar, A. & Bozovic, I. High–temperature superconductivity in a single copper–oxygen plane. *Science* **326**, 699–702 (2009).
14. Bollinger, A. T., Dubuis, Yoon , G. J., Pavuna, D., Misewich, J. & Bozovic, I. Superconductor–insulator transition in $La_{2-x}Sr_xCuO_4$ at the pair quantum resistance. *Nature* **472**, 458–460 (2011).
15. Hansmann, P., Yang, X. P., Toschi, A., Khaliullin, G., Andersen, O. K. & Held, K. Turning a nickelate fermi surface into a cupratelike one through heterostructuring. *Phys. Rev. Lett.* **103**, 016401 (2009).
16. Hansmann, P., Toschi, A., Yang, X. P., Andersen, O. K. & Held, K. Electronic structure of nickelates: From two-dimensional heterostructures to three-dimensional bulk materials. *Phys. Rev. B* **82**, 235123 (2010).
17. Yang, X. P. & Su, H. Polarization and electric field dependence of electronic properties in $LaAlO_3/SrTiO_3$ heterostructures. *ACS Appl. Mater. Interfaces* **3**, 3819–3823 (2011).
18. Yang, X. P. & Su, H. Electronic reconstruction and surface two-dimensional electron gas in a polarized heterostructure with a hole-doped single copper-oxygen plane. *Phys. Rev. B* **87**, 205116 (2013).
19. Kresse, G. & Hafner, J. Ab initio molecular dynamics for liquid metals. *Phys. Rev. B* **47**, 558–561 (1993).
20. Kresse, G. & Hafner, J. Ab initio molecular–dynamics simulation of the liquid–metal–amorphous–semiconductor transition in germanium. *Phys. Rev. B* **49**, 14251–14269 (1994).
21. Kresse, G. & Furthmüller, J. Efficient iterative schemes for ab initio total–energy calculations using a plane–wave basis set. *Phys. Rev. B* **54**, 11169–11186 (1996).
22. Kresse, G. & Furthmüller, J. Efficiency of ab–initio total energy calculations for metals and semiconductors using a plane–wave basis set. *Comput. Mater. Sci.* **6**, 15–50 (1996).
23. Perdew, J. P., Burke, K. & Ernzerhof, M. Generalized gradient approximation made simple. *Phys. Rev. Lett.* **77**, 3865–3868 (1996).
24. Marzari, N. & Vanderbilt, D. Maximally localized generalized Wannier functions for composite energy bands. *Phys. Rev. B* **56**, 12847–12865 (1997).
25. Souza, I., Marzari, N. & Vanderbilt, D. *Phys. Rev. B* **65**, 035109 (2001).
26. Mostofi, A. A., Yates, J. R., Lee, Y.-S., Souza, I., Vanderbilt, D. & Marzari, N. Wannier90: A tool for obtaining maximally–localised wannier functions. *Comput. Phys. Commun.* **178**, 685–699 (2008).
27. Kresse, G. & Joubert, D. From ultrasoft pseudopotentials to the projector augmented-wave method. *Phys. Rev. B* **59**, 1758–1775 (1999).
28. Blöchl, P. E. Projector augmented–wave method. *Phys. Rev. B* **50**, 17953–17979 (1994).
29. Anisimov, V. I., Zaanen, J. & Andersen, O. K. Band theory and Mott insulators: Hubbard U instead of Stoner I. *Phys. Rev. B* **44**, 943–954 (1991).
30. Weber, C., Yee, C.-H., Haule, K. & Kotliar, G. Scaling of the transition temperature of hole–doped cuprate superconductors with the charge–transfer energy. *EPL* **100**, 37001 (2012).

Acknowledgments

We are grateful for the interesting discussions with T. Maurice Rice, Bill Goddard, Fuchun Zhang, Haiqing Lin, Hans Hilgenkamp, Jaichan Lee, Adrian Gozar, and Daoxin Yao. This work was supported in part by the A*STAR SERC grant (no. 1121202012, 1223600006).

Author contributions

H.B.S. conceived the project. X.P.Y. performed the calculations. All authors discussed the results, wrote and commented on the manuscript at all stages.

Additional information

Supplementary information accompanies this paper at http://www.nature.com/scientificreports

Competing financial interests: The authors declare no competing financial interests.

How to cite this article: Yang, X. & Su, H. Cuprate-like Electronic Properties in Superlattices with $Ag^{II}F_2$ Square Sheet. *Sci. Rep.* **4**, 5420; DOI:10.1038/srep05420 (2014).